Composites: Part B 53 (2013) 17–24

Contents lists available at SciVerse ScienceDirect

Composites: Part B

journal homepage: www.elsevier.com/locate/compositesb

Bending analyses for 3D engineered structural panels made from laminated paper and carbon fabric

Jinghao Li [a,b], John F. Hunt [b,*], Zhiyong Cai [b], Xianyan Zhou [a]

[a] College of Civil Engineering and Mechanics, Central South University of Forest and Technology, Changsha 410004, China
[b] USDA Forest Service, Forest Products Laboratory, Madison, WI 53726, United States

ARTICLE INFO

Article history:
Received 19 October 2012
Received in revised form 14 March 2013
Accepted 12 April 2013
Available online 21 April 2013

Keywords:
A. Laminates
A. Carbon fiber
C. Finite element analysis (FEA)
D. Mechanical testing

ABSTRACT

This paper presents analysis of a 3-dimensional engineered structural panel (3DESP) having a tri-axial core structure made from phenolic impregnated laminated-paper composites with and without high-strength composite carbon-fiber fabric laminated to the outside of both faces. Both I-beam equations and finite element method were used to analyze four-point bending of the panels. Comparisons were made with experimental panels. In this study, four experimental panels were fabricated and analyzed to determine the influence of the carbon-fiber on bending performance. The materials properties for finite element analyses (FEA) and I-beam equations were obtained from either the manufacturer or in-house material tensile tests. The results of the FEA and I-beam equations were used to compare with the experimental 3DESP four-point bending tests. The maximum load, face stresses, shear stresses, and apparent modulus of elasticity were determined. For the I-beam equations, failure was based on maximum stress values. For FEA, the Tsai-Wu strength failure criterion was used to determine structural materials failure. The I-beam equations underestimated the performance of the experimental panels. The FEA-estimated load values were generally higher than the experimental panels exhibiting slightly higher panel properties and load capacity. The addition of carbon-fiber fabric to the face of the panels influenced the failure mechanism from face buckling to panel shear at the face–rib interface. FEA provided the best comparison with the experimental bending results for 3DESP.

Published by Elsevier Ltd.

1. Introduction

Sandwich panels are used for a variety of applications including those for building, transportation, furniture, decking, packaging, marine, and aerospace. Marine and aerospace applications have the most demanding performance requirements and use the highest strength materials. Many of these sandwich panels are fabricated using honeycomb construction for the core structure. However, over the past 15 years, researchers have shown a new interlocked composite grid arrangement that could offer improved performance for some applications [1,2]. The interlocking grid uses linear ribs that are double-slotted for 1/3 the width or single-slotted for 2/3 the width of the rib. The double-notched ribs were used as the main rib orientation and the 2/3 notched ribs are inserted from either the top or bottom side to create a triangular core design (Fig. 1). According to Fan et al, this core configuration has been shown to be stiffer and stronger than foams and honeycombs [3]. The size of the equilateral triangle shown could be modified by adjusting the distance between slots or changing the design to an isosceles triangle by adjusting the distances between slots for the double-slotted rib, thus creating a core with performance options that can be engineered.

This study was initiated to investigate the performance characteristics for this core structure as it relates to wood-fiber-based composite materials. An integrated equivalent stiffness model was developed to describe the grid structure with consideration of multiple loads, multiple failure mechanisms, and design variations as outlined by Chen and Tsai [1] but using wood-based composite materials.

The Forest Products Laboratory (FPL) is working to develop 3-dimensional engineered structural panels (3DESPs) made from a significant portion of wood-based composite materials yet that have enhanced performance capabilities. For some applications, high-performance and water resistance are critical requirements but do not have the same high performance or weight requirements as marine or aerospace panels. It may be possible that a phenolic impregnated laminated paper might be sufficient to fill some niche applications at slightly reduced costs. The laminated paper was used to fabricate the tri-axial rib core components and the initial top and bottom faces. The lower cost laminated paper faces were also used to support a thinner yet higher MOE carbon-fabric

* Corresponding author. Tel.: +1 608 231 9433.
E-mail address: jfhunt@fs.fed.us (J.F. Hunt).

1359-8368/$ - see front matter Published by Elsevier Ltd.
http://dx.doi.org/10.1016/j.compositesb.2013.04.041

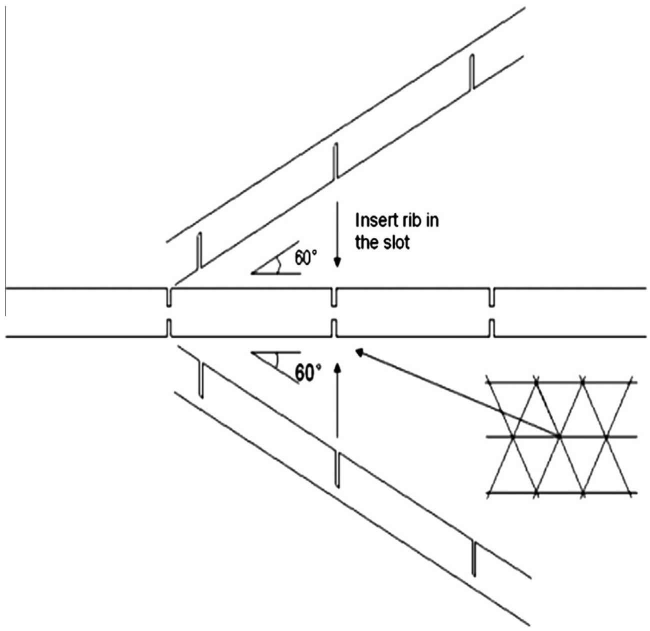

Fig. 1. Fabrication of tri-axial core or isogrid structure from linear material.

material. The thin single layer of carbon fabric would have easily buckled across the widely spaced ribs during bending, but by laminating the paper laminate and carbon fabric together achieved a high stiffness panel structure.

This work is a preliminary experiment to evaluate the bending performance of 3DESP. For the experiment, the bending failure, deflection, and bending stress were evaluated using numerical and finite element analyses (FEA). Also, the 3DESP experimental and FEA results were compared with traditional I-beam theory.

2. Theoretical approach

2.1. I-beam equations

Conventional I-beam equations were used to estimate the quarter-point beam bending performance for the tri-axial core 3DESP. The face and rib tension/compression stress, shear stress, and deflection were determined using standard strength of materials for bending [4].

2.2. Finite element method for plane elements

ANSYS FEA software (ANSYS, Inc., Canonsburg, Pennsylvania, USA) [5,6], was used to model the core and face using their eight-node quadrilateral shell element, Shell 99. The virtual work equation is given by the following equation [6]:

$$\int\int\int_V \delta\{\varepsilon\}^T\{\sigma\}dV - \int\int_V \delta\{u\}^T\{T\}dS = 0 \tag{1}$$

In this equation, $\{\varepsilon\}$, $\{\sigma\}$, $\{T\}$, $\{u\}$, V, and S represent strain, stress, displacement, applied load, volume, and area, respectively.

Linear small strains were assumed in this study, the matrix equation is given by

$$\{\varepsilon\} = [B]\{u\} \tag{2}$$

where $[B]$ represents the strain matrix.

The relationship between stress and strain in the structural panel is given by the following equation

$$\{\sigma\} = [Q]\{\varepsilon\} \tag{3}$$

where $[Q]$ is the stiffness matrix in the equation.

The results were obtained by substituting Eqs. (2) and (3) into (1).

2.3. Failure criterion

The Tsai-Wu failure criterion is a commonly used material failure criterion for composite materials. In this paper, Tsai-Wu failure criterion was applied to estimate the maximum failure load on materials by FEA. The quadratic Tsai-Wu failure criterion was given by the following equation [7]:

$$f_1\sigma_1 + f_2\sigma_2 + f_{11}\sigma_1^2 + f_{22}\sigma_2^2 + f_{66}\sigma_6^2 + 2f_{12}\sigma_1\sigma_2 \geq 1 \tag{4}$$

where σ_1 and σ_2 are stresses along the longitudinal (Machine direction (MD)) and transverse (Cross direction (CD)) directions, respectively. Shear stress, σ_6, is the in-plane shear stress. The strength parameters f_1, f_2, f_{11}, f_{22}, f_{66}, and f_{12} are given by the following equations:

$$f_1 = \frac{1}{F_{1t}} - \frac{1}{F_{1c}},\ f_{11} = \frac{1}{F_{1t}F_{1c}},\ f_2 = \frac{1}{F_{2t}} - \frac{1}{F_{2c}},\ f_{22} = \frac{1}{F_{2t}F_{2c}},\ f_{66} = \frac{1}{F_6^2} \tag{5}$$

where F_{1t} is the tensile strength in MD (Pa); F_{1c} is compressive strength in MD (Pa); F_{2t} is the tensile strength in CD (Pa); F_{2c} is compressive strength in CD (Pa); and F_6 is the shear strength (Pa). The interaction coefficient f_{12} is approximated by

$$f_{12} = -\frac{1}{2}\sqrt{f_{11}f_{22}} \tag{6}$$

The Tsai-Wu failure criterion identifies an element failure. The FE analyses of the bending test used the Tsai-Wu failure criterion to calculate the max failure load for elements of the structural panels.

3. Material properties

The material properties used for this study were obtained from either the manufacturer or by material testing according to ASTM test methods D229, D638, and D695 [8–10]. The material properties for the individual components are provided in Table 1. Phenolic impregnated laminated paper NP610, Norplex-Micarta Inc. (Postville, Iowa, USA), was used for the core and faces. The laminated paper had orthogonal properties designated MD and CD. Carbon fiber fabric, a tri-axial woven material, QISO, was obtained from A&P Technology (San Jose, California, USA). It was bonded to the outside layer of the laminated paper faces of the 3DESP using U.S. Composites (West Palm Beach, Florida, USA) epoxy, 635. The ratio of epoxy to hardener was 3:1. The laminated paper was tested by itself and then with carbon-fiber fabric bonded one side. The properties for the carbon-fiber fabric /epoxy resin composite by itself were difficult to obtain because of weave separation rather than tensile failure. Therefore, the carbon-fiber fabric was bonded first to the laminated paper and then the composite was tested in MD and CD. Machine direction is defined as the primary direction the laminates were fabricated, and generally the MD mechanical properties are greater than the CD. The laminated paper bonded with the carbon-fiber fabric was used to provide better combined test values for the material properties than using individual material properties. The tensile properties were obtained using dogbone shaped specimens. Poisson's ratios υ_{xy} and υ_{xz} were also obtained from standard tensile tests measuring both axial and transverse strains. Epoxy shear strength was determined according lap-shear test method ASTM D5868 [11]. The average epoxy shear strength was 17.9 MPa between the laminated paper.

Table 1
Materials properties of 3DESP.

Materials	Material properties								
	Nominal thickness (mm)	Density (kg/m^3)	Comp. strength (MPa)	Tensile strength MD[a] (MPa)	Tensile strength CD[b] (MPa)	MOE MD (GPa)	MOE CD (GPa)	Poisson ratios in MD[a]	Poisson ratios in CD[b]
Laminated paper (LP)	2.36	1387	241	173.9	118.6	11.6	8.3	0.36	0.22
Carbon fiber/ LP[c]	3.15	1354	241	216.6	132.2	16.3	13.6	0.36	0.46
Epoxy resin	–	1101	105.9	31.0	–	1.4	–	0.42	–

[a] MD is machine direction.
[b] CD is cross-machine direction.
[c] Carbon fiber bonded with laminated paper composite.

4. The experimental design and finite element models for bending test

The 3DESPs were constructed with the tri-axial core configuration using laminated paper for its linear ribs in each of the three axes (Fig. 1). The core or linear rib height was 33.0 mm. The slots in the core pieces were cut slightly oversized to account for the 60° angular orientation between parts when assembled. The distance between slots for all pieces was 117.3 mm, thus creating an equilateral triangle. The double-slotted linear ribs aligned with the MD of the laminated paper. The laminated paper faces were first lightly sanded on one side and epoxy resin applied to the sanded surface. Then the core was placed on the surface with epoxy. The panels that had the carbon-fiber fabric applied to the outside surfaces were also sanded prior to application of the epoxy and the carbon-fiber fabric. The primary alignment for the carbon-fiber fabric aligned with the MD of the laminated paper.

Four-point bending test method, ASTM C393 [12], was used to test the panels. The panels were fabricated and cut so the ribs were centrally located and included three complete linear ribs. After testing three of the panels, we found that for the reaction points were not equidistant from the loading head. This off-center configuration was addressed using the general equations for off-center loading. The set-up was corrected for the fourth panel tested (ID No. 1). The test set-up dimensions for each panel are listed in Table 2.

Experimental panels 1 and 2 were made with laminated paper faces only. Panels 3 and 4 were made with carbon fiber bonded to the laminated paper faces. The same core dimensions were used for all panels. The test loading set-up is shown in Fig. 2.

ANSYS FEA software [13] was used to model the 3DESP. Properties and dimensions for the models are listed in Tables 1 and 2. The eight-node shell element, Shell 99, was used to analyze the structure. Approximately 20,000 elements were used to mesh the models. The reaction points were held in-place and load applied at the same location as the actual 3DESP panels. The decision tree shown in Fig. 3 was used to analyze the mechanical and failure mechanism of the 3DESP. Tsai-Wu failure criteria (Eq. (4)) needs to be equal to or greater than 1 for the FEA simulation to quit; otherwise, the FEA continued to increase load to induce failure.

5. Results and Discussion

5.1. Panel failure mode

Fig. 4 shows two types of bending failure observed for the 3DESP. For the laminated paper panels, panels 1 and 2, both failures were on the compression side between the mid-span of the loading bars. Under test load but prior to failure, the compression face showed signs of out-of-plane displacement. It is unknown what failure mode initiated the brittle failure of the compression side face, but it could have been either compression buckling of the core ribs or out-of-plane buckling of the face. Either could have been initiated as stresses approached material maximums. It is most probable that failure was initiated from face buckling causing localized bending or buckling of the core beneath the load point resulting in a surface fracture. Post-failure observation of the panels showed there were no noticeable epoxy shear failure between the face and ribs.

For panels 3 and 4 with the added layers of carbon-fiber fabric to both sides of the panel, there was no noticeable out-of-plane buckling of the faces. The failure mode shifted from face buckling failure to shear failure at the resin interface between the ribs and faces between the inner and outer spans of the panel.

5.1.1. Panels 1 and 2: load vs. deflection results

Figs. 5–8 are plots of load vs. mid-point deflection for panels 1, 2, 3, and 4, respectively. For each figure are three plots: 1. Simplified I-beam theory, 2. FEA, and 3. Experimental tests. The simplified I-beam responses were based on standard quarter-point bending equations that are linearly related to the load and do not consider any non-linear responses from the material. The simplified equations only included the ribs parallel with the long panel direction and did not consider any load-carrying contribution from the off-axis ribs. Failure was based on the maximum

Table 2
Dimension of panels for 3DESP bending testing.

Experimental panel ID (No.)	Test setup dimensions				
	Span of beam *L* (mm)	Load distance *a* from support R1 (mm)	Load distance *b* from support R2 (mm)	The thickness of beam (mm)	The width of beam (mm)
1	914	305	305	38.1	267
2	1057	345	358	38.1	277
3	1057	345	358	39.6	254
4	1057	345	358	39.6	305

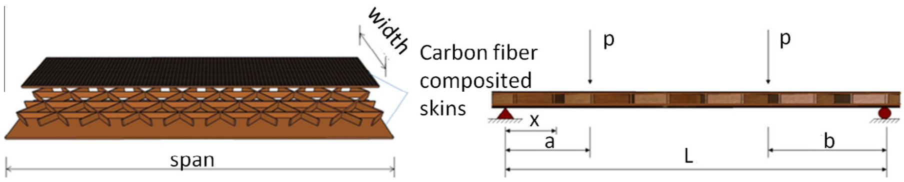

Fig. 2. 3DESP construction and test set-up for four-point bending.

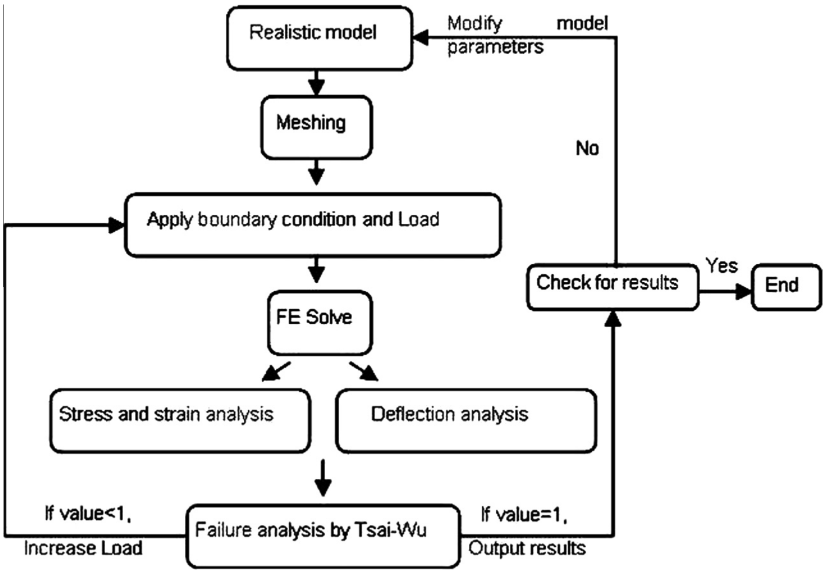

Fig. 3. Flow chart of the finite element analyses.

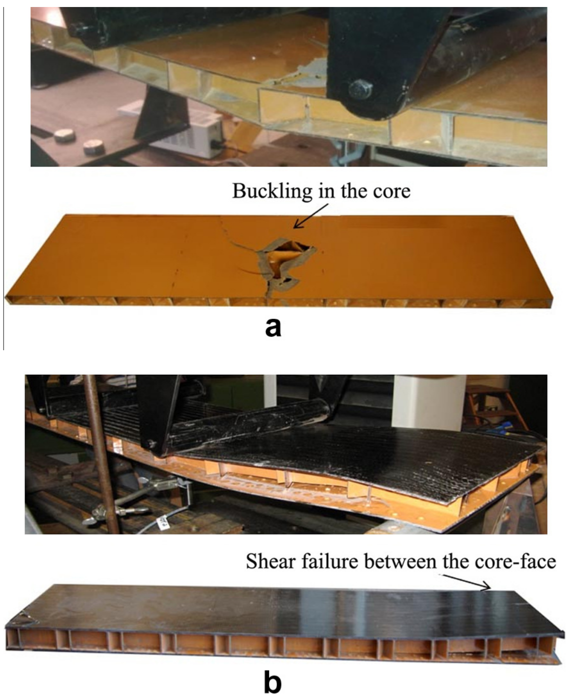

Fig. 4. (a) Laminate paper 3DESP bending failure caused by brittle compression of the face. (b) Carbon-fiber fabric 3DESP bending failure caused by shear between core and bottom face.

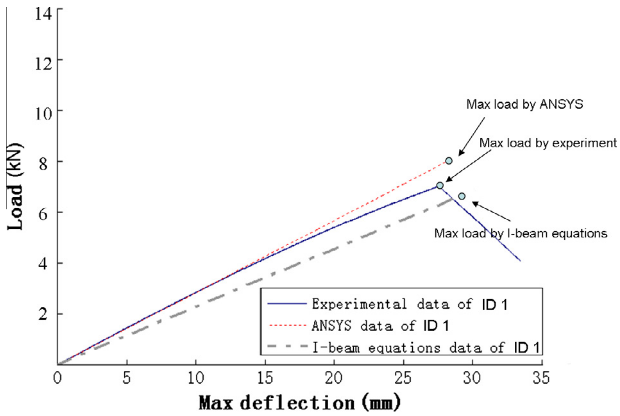

Fig. 5. The relationship between load and max deflection for panel 1.

tension/compression stress in the faces or maximum shear stress of the epoxy at the face–rib interface. Buckling equations for the faces were not applied for this study because of the complexity of the loading conditions. The lower of either the tensile/compression face stress of 173.9 MPa, Table 1, or maximum epoxy shear stress of 17.9 MPa were used to estimate the potential load capacity for the panels. For the FEA models, perfect bonding between components was assumed and the Tsai-Wu failure criteria (Eq. (4)) was used and failure was assumed to occur at any point in the panel when the total value exceeded 1.0. The maximum epoxy

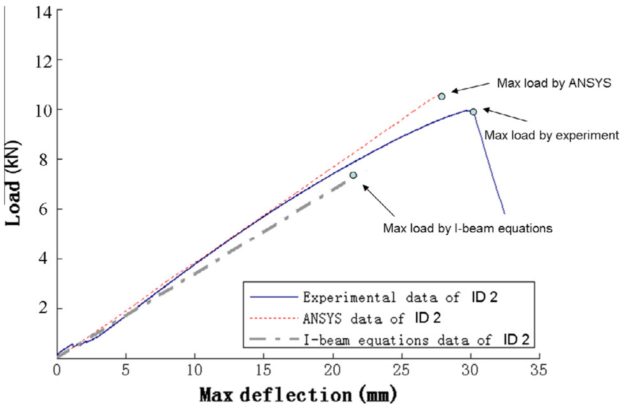

Fig. 6. The relationship between load and max deflection for panel 2.

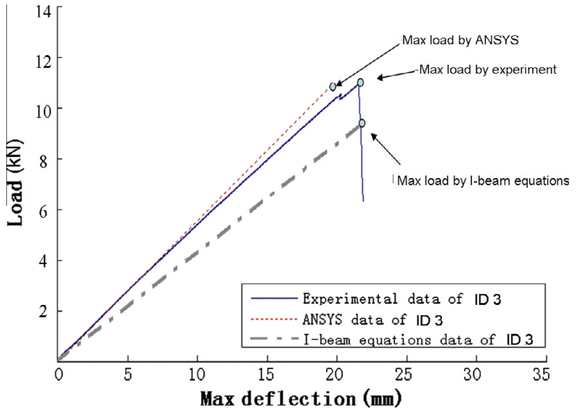

Fig. 7. The relationship between load and max deflection for panel 3.

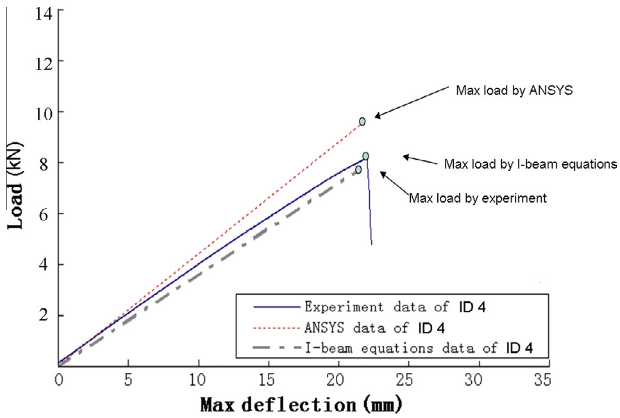

Fig. 8. The relationship between load and max deflection for panel 4.

shear failure stress criteria at the face–rib interface was also considered for the FEA models. The actual experimental plots for each panel are shown for comparison.

Using the simplified I-beam theory, estimated maximum loads for panels 1 and 2 were 6.5 and 7.2 kN, respectively (Table 3) when the maximum face stress reached 173.9 MPa. The maximum face stresses were located between the mid-span load points. The calculated shear stress at the maximum loads were 13.8 and 15.6 MPa, which were less than the 17.9 MPa allowable epoxy shear stress. The calculated loads were less than the actual loads partially because (a) The equations do not account for the load-carrying capacity from the off-axis ribs or (b) The lower of either tension or compression stresses was used to calculate estimated failure load. Compression stresses were calculated to be higher than tension stresses in the panel.

FEA-estimated failure loads for panels 1 and 2 occurred at 8.0 and 10.7 kN, respectively. As FEA can account for most stress conditions within the structure, Tsai-Wu failure criteria was used to calculate when the combined stresses (Eq. (4)) exceeded 1.0. Based on Tsai-Wu criteria, the failure load for the combined stresses occurred in the ribs beneath the loading points mid-way between the two faces. The maximum face stresses at that failure criteria were 126.4 and 159.3 MPa, respectively. These were less than the estimated face stresses calculated using the simplified equations. The maximum shear stresses of 17.6 and 24.1 MPa were located in the rib but not at the face–rib interface, so the maximum of 17.9 MPa epoxy shear failure did not apply. The maximum FEA failure stresses occurred beneath the load points. We believe this is where failure initiated followed by buckling/tension failure of the faces as observed for the experimental panels.

Experimental failure loads for panels 1 and 2, were 7.0 and 9.9 kN, respectively. These failure loads were then plugged back into the FEA models to calculate estimated maximum face stresses and maximum shear stresses (Table 3). The estimated maximum face stresses were 112.8 and 148.1 MPa and estimated maximum shear stresses were 15.4 and 22.4 MPa, respectively. The estimated maximum face stresses of panels 1 and 2 were both located under the loading area and the maximum shear stresses of panels 1 and 2 were both located beneath the supported sections of axis ribs. The maximum shear stresses at the face–rib interface were 10.5 MPa and 14.2 MPa, respectively, near the supports. These shear stresses were less than the shear property of epoxy resin; therefore, failure did not occur from shear stress but the panels failed because of face buckling.

5.1.2. Panels 3 and 4: load vs. deflection results

For the carbon-fiber fabric covered panels, 3 and 4, the failure criteria for both the I-beam equations and the FEA was assumed to be epoxy shear failure at the face–rib interface between the inner load and outer reaction points. For a four-point bending test, shear stress was assumed constant between the reaction and the loading points. Using the maximum shear stress values for the epoxy, the estimated maximum loads would be 9.4 and 7.8 kN, respectively. In addition, face stresses calculated for the area between the inner load points were both 173.7 MPa, respectively (Table 2). This stress level was less than the 216.6 MPa (Table 1) maximum measured tensile stress for the carbon-fiber fabric / laminated paper composite. For the FEA analyses, the maximum loads were determined to be 10.5 and 9.6 kN, respectively. At these loads, the maximum face stresses would be 107.9 and 115.7 MPa, respectively. This was much lower than the 173.7 MPa calculated by Eq. (1) and were also half the material failure stress. The main difference between the beam equations and FEA is that FEA included the off-axis rib material in the analyses, whereas the simplified equations only use the linear ribs in the analyses. FEA clearly showed that the carbon-fiber fabric provided increased support to the faces to prevent localized face buckling and reduced faces stresses (Fig. 9). The experimental failure loads were 10.9 and 8.2 kN. These failure loads were used as inputs in ANSYS to determine the face–rib interface stresses. The interface stress maximums were 18.4 and 15.0 MPa, respectively. It is possible the low panel load value of 8.2 MPa was due to face–rib epoxy bonding defect that caused premature shear failure at the lower 15.0 MPa.

In all cases, the simplified equations estimated lowest panel loads compared with those from the FEA or the experimental tests.

Table 3
Panel mechanical properties.

Panel ID	Failure loads											
	Maximum load, kN (% Change from Experimental)			Apparent Panel modulus of elasticity, GPa (% Change from experimental)			Maximum face stress, MP[a] (% Change from experimental)			Maximum shear stress, MPa (% Change from experimental)		
	Equation[a]	FEA[b]	Experimental[c]	Equation	FEA	Experimental	Equation	FEA	Experimental	Equation	FEA	Experimental
1	6.5 (−7)	8.0 (14)	7.0	9.8 (−21)	12.2 (−2)	12.4	173.9 (54)	126.4 (12)	112.8	13.8 (−10)	17.6 (14)	15.4
2	7.2 (−27)	10.7 (8)	9.9	9.8 (−21)	11.1 (−10)	12.4	173.9 (17)	159.3 (8)	148.1	15.6 (−30)	24.1 (8)	22.4
3	9.4 (−14)	10.5 (−4)	10.9	12.7 (−21)	16.3 (1)	16.1	173.7 (56)	107.9 (−3)	111.3	17.9 (−3)	17.9 (−3)	18.4
4	7.8 (−5)	9.6 (17)	8.2	12.7 (−9)	15.6 (12)	13.9	173.7 (75)	115.7 (17)	99.2	17.9 (19)	17.9 (19)	15.0

[a] The maximum load of Equation was estimated by maximum stress of materials.
[b] The maximum load of finite element analysis (FEA) was estimated by Tsai-Wu criterion in ANSYS based on material properties.
[c] The maximum stress and MOE of experimental was estimated by ANSYS based on experimental maximum load.

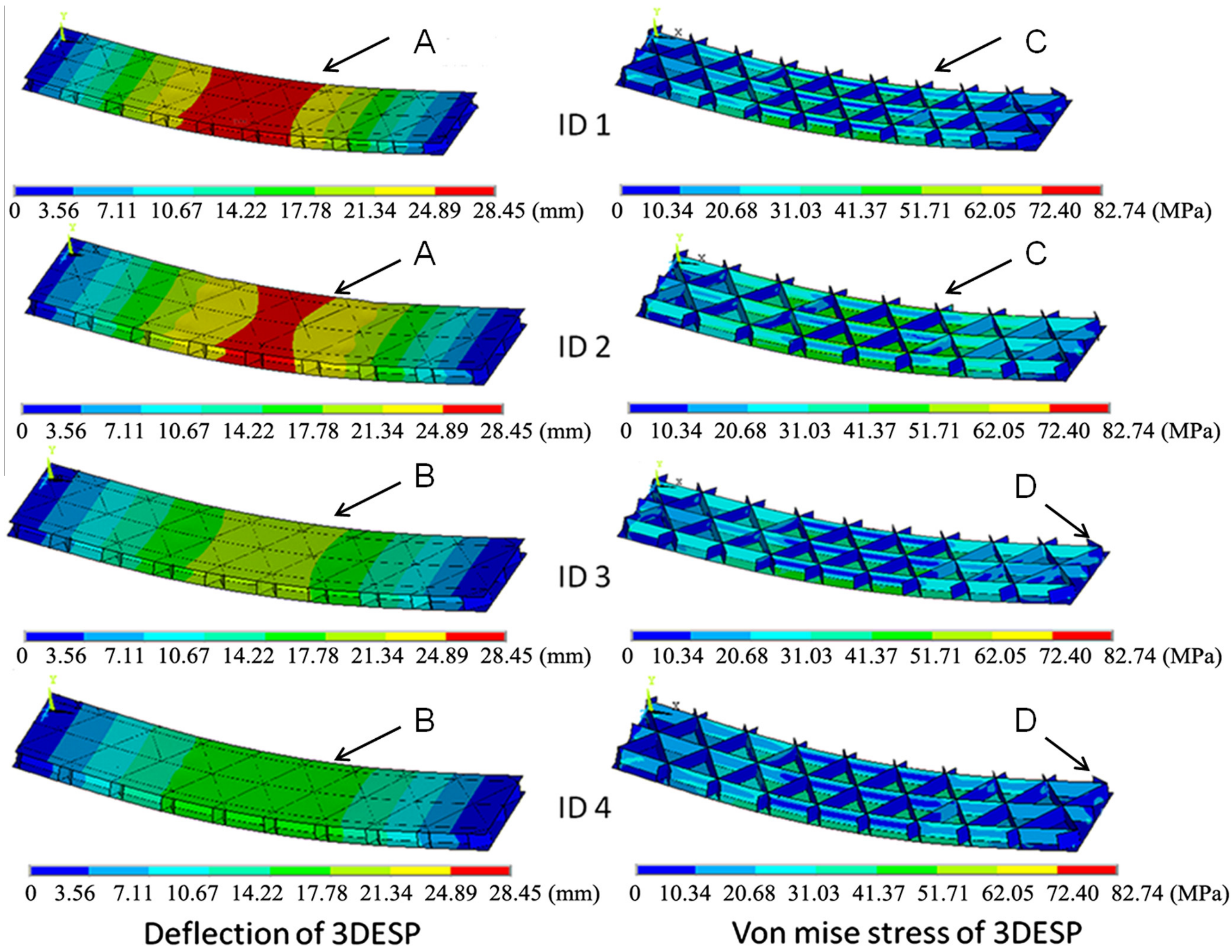

Fig. 9. The deflection and von mise stress for panels 1–4 based on their estimated max load. (A) Large out-of-plane deformation in mid-span area between the ribs; (B) Small out-of-plane deformation in the mid-span area between the ribs; (C) Max stress on both top and bottom next to skins between mid-span area; (D) Max shear stress at the support area between the core and skins.

This may have been due in part to the simplistic assumptions of only having linear ribs rather than two additional supporting ribs in the off-axis directions. FEA resulted in the highest panel load capacity except for panel 3 where the experimental panel must have had slightly better face–rib shear support to achieve higher shear strength. The extra shear strength resulted with the highest panel load. In general, however, the FEA assumes perfect bonding and therefore resulted in higher load capacities. The estimated loads using the I-beam equations were 7, 27, 14, and 5% less, respectively, than the experimental results. The FEA estimated panel loads were 14, 8, −4, and 17%, respectively, greater than the experimental results. Better FEA models that include a resin layer at the face–rib interface, and better fabrication techniques would help to reduce the differences.

5.2. Panel mechanical properties

All the experimental panels exhibited relatively linear load vs. deflection curves (Figs. 5–8) indicating a predominant elastic response to load. They were assumed to be linear so only the elastic part of the beam deflection equation was used to determine panel stiffness. The maximum load and deflection obtained from the experimental test and the estimates from the FEA analysis and the simple equation were then used to determine panel stiffness from the elastic portion of the ASTM C393 test method. An apparent MOE was then calculated for each panel, obtained by dividing the stiffness by the area moment of inertia from each panel's sectional dimensions. Comparing panel apparent MOE values (Table 3), the results from the I-beam equations were the lowest of all the panels. The equations predicted an apparent moduli that were 21, 21, 21, and 9% less, respectively, than the experimental results. Again, we believe this was due in part to the off-axis components that were not accounted for with the simplified calculations. For FEA, apparent panel MOE values were very close to the experimental values being only 2 and 10% less for panels 1 and 2, respectively. The FEA could better account for the effects of the off-axis ribs than the I-beam equations. Initial stiffness for all the experimental panels were initially fairly linear; however, as load increased non-linear behavior can be observed. It can be seen that the FEA responses were linear elastic and consistently higher than the experimental. The FEA apparent MOE values for panels 3 and 4 were 2 and 11% greater than the experimental panels. The FEA model assumed perfect bonding at the face–rib interface; however, the failed experimental panels, 3 and 4, showed areas where the epoxy did not provide adequate shear bonding. Poor bonding would have resulted in lower experimental apparent MOE values. Improved fabrication techniques most likely would have increased the experimental properties. Also, the FEA models assumed laminated paper-to-laminated paper connection and did not model the epoxy material properties in the face–rib interface. Placing the epoxy into the evaluation would have decreased the stiffness slightly, which will be checked in future analyses. Fig. 9 shows FEA shear stress along the length of the linear ribs between the rib and face. Shear stress along the interface was not uniform and the model did show shear decreased at the intersection of the ribs and increased between intersections, as expected.

Fig. 9 shows the deflection and von mise stresses for each panel at the maximum experimental load. For panels 1 and 2, the faces showed larger asymmetrical deflections than panels 3 and 4. Panels 1 and 2 were slightly thinner than the carbon-fabric panels 3 and 4, because of the carbon-fiber fabric layers on top and bottom faces. The added carbon-fiber fabric significantly increased the average face material MOE from 173.9 to 216.6 MPa, a 24% increase. For both models, equation and FEA, the increased composite face MOE and increased panel thickness added to the overall apparent MOE for panels 3 and 4. For the I-beam equations, the panel apparent MOE increased by almost 30% and the apparent MOE for the FEA panels increased by almost 37%. Localized face buckling was reduced with the increased face thickness, which is also evident when comparing panels 1 and 2 with 3 and 4 (Fig. 9). It is also interesting to note that the stiffer and stronger carbon-fabric panels shifted failure to shear at the face–rib interfaces between the outer reaction points and the inner load point. Shear free-body diagrams for this beam set-up would assume constant shear through this area. The FEA model was also used to look at the interface shear stress and was found to be non-uniform along the length of the ribs. Higher stresses were found at the intersection points and less between the intersections. Maximum shear occurred at the outer reaction points (Fig. 9).

For optimized carbon-fabric panel design, either decrease carbon-fiber fabric thickness a little so face stresses might match bending face stress or increase core shear capacity at the face to core interface. Increased core shear capacity could be obtained by increasing the number of ribs, increasing the thickness of the ribs, or provide shear fillets at the face–rib interface.

6. Conclusions

The design of the 3DESP structure can be conservatively analyzed with I-beam equations, but FEA evaluation provides better analyses of the potential performance or potential failures as exhibited by the experimental tests. The effect of adding carbon-fiber fabric showed significant improvement in overall stiffness and shifting of buckling failure stresses from the faces between the load span to shear between loading and reaction points. By knowing where maximum stresses occur in the panel, it is possible to optimize the design and reduce failure stresses to improve performance. This shows it is possible to design for optimal stiffness and failure based on material properties using the tri-axial core design. Depending on the failure mechanism, the equations could be used to predict reasonable conservative values.

The additional stiffening effect of the carbon fiber fabric when combined with the laminated paper provided improved load distribution through the faces onto the core ribs. The addition of QISO fabric increased thickness of the faces that helped to carry the load over a wider area thus reducing the potential of buckling for the ribs.

The FEA adequately modeled the performance of the 3DESP off-axis rib alignment. The faces with the carbon-fiber fabric did not reach compressive or tensile failure loads but failed in shear. Future studies will look at increasing shear capacity in the core to see if failure can be pushed back to compression or tension of the faces. Shear failure at the face–rib interface indicates over-design of the faces or under-design of the core. Both design considerations will be analyzed in future papers. FEA modeling was also effective in modeling rib buckling that may have led to face compression failure.

Acknowledgment

This work is supported by USDA Forest Products Laboratory and Plan Projects of Introducing Advanced International Forestry Technology (2010-4-14).

References

[1] Chen HJ, Tsai SW. Analysis and optimum design of composite grid structures. J Compos Mater 1996;30(4):503–34.
[2] Han DY, Tsai SW. Interlocked composite grids design and manufacturing. J Compos Mater 2003;37(4):287–316.
[3] Fan HL, Meng FH, Yang W. Sandwich panels with kagome lattice cores reinforced by carbon fibers. Compos Struct 2007;81:533–9.
[4] Sun XF. Material Mechanics. Hong Kong: Higher Education Publishing House; 2002.
[5] ANSYS. Finite Element Software. Canonsburg, Pennsylvania, 2004.
[6] Ding K. Finite Element Method. Peking University Press; 2006.
[7] Tsai SW, Wu EM. A general theory of strength for anisotropic materials. J Compos Mater 1971;5(1):58–80.

[8] ASTM. Standard D229-09. Standard test methods for rigid sheet and plate materials used for electrical insulation. American Society for Testing and Materials. West Conshohocken: Pennsylvania; 2009.
[9] ASTM. Standard D638-10. Standard test method for tensile properties of plastics. American Society for Testing and Materials. West Conshohocken: Pennsylvania; 2010.
[10] ASTM. Standard D695-10. Standard test method for compressive properties of rigid plastics. American Society for Testing and Materials. West Conshohocken: Pennsylvania; 2010
[11] ASTM. Standard D5868–01. Standard Test Method for Lap Shear Adhesion for Fiber Reinforced Plastic (FRP) Bonding. West Conshohocken: Pennsylvania; 2001.
[12] ASTM. Standard C393–00. Standard Test Method for Flexural Properties of Sandwich Constructions American Society for Testing and Materials. West Conshohocken: Pennsylvania; 2000.
[13] ANSYS. Finite Element Software. ANSYS, Inc., Canonsburg: Pennsylvania; 2004.